Analytical Methods

Accepted Manuscript

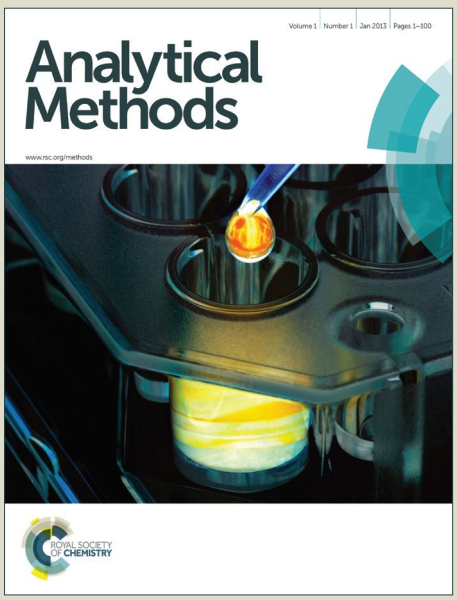

This is an *Accepted Manuscript*, which has been through the Royal Society of Chemistry peer review process and has been accepted for publication.

Accepted Manuscripts are published online shortly after acceptance, before technical editing, formatting and proof reading. Using this free service, authors can make their results available to the community, in citable form, before we publish the edited article. We will replace this *Accepted Manuscript* with the edited and formatted *Advance Article* as soon as it is available.

You can find more information about *Accepted Manuscripts* in the Information for Authors.

Please note that technical editing may introduce minor changes to the text and/or graphics, which may alter content. The journal's standard Terms & Conditions and the Ethical guidelines still apply. In no event shall the Royal Society of Chemistry be held responsible for any errors or omissions in this *Accepted Manuscript* or any consequences arising from the use of any information it contains.

ROYAL SOCIETY OF CHEMISTRY

www.rsc.org/methods

Seaweed-polyaniline nanofibre modified electrode for sensing of uric acid

Ramasamy Pandimurugan, Sivalingam Thambidurai*

Department of Industrial Chemistry, School of Chemical Sciences, Alagappa University, Karaikudi 630003, Tamil Nadu, India.

Abstract: In this paper, seaweed-polyaniline (SE-PANI) nanofibe were prepared through a polymerization of aniline hydrochloride in the presence of seaweed extract (SE) and ammonium persulphate (APS) used as an oxidant. The resultant SE-PANI nanofibre were characterized by different techniques such as Fourier transform infrared spectroscopy, Ultra violet-visible spectroscopy, X-ray diffraction, High resolution scanning electron microscopy and Brunauer–Emmett–Teller analysis. Thermal stabilities of the SE-PANI nanofibre were higher than pristine PANI confirmed by thermogravimetric analysis and differential thermal analysis. The electrochemical measurements SE-PANI nanofibre was studied by cyclic voltammetry and electro-chemical impedance spectroscopy. SE-PANI/GCE modified electrode shows a better electro catalytic activity for uric acid (UA) with lower potential and large peak current than pristine PANI modified glassy carbon electrode. DPV studies revealed that the fabricated electrode had excellent sensitivity for uric acid with the lowest detection limit of 0.104 μM over a wide concentration range of 5×10^{-5} to 5×10^{-3} M.

Keywords*:* Polyaniline; biopolymers; nanofibre; morphology; cyclic voltammetry; DPV.

Email: sthambi01@yahoo.co.in (S.Thambidurai)

Tel.: +91 4565 228836; fax: +91 4565 225202.

1. Introduction

Uric acid (UA) is a major final product of urine metabolism, in a healthy human body present in biological fluids like blood and urine. Anomalous levels of UA would causes several disorders including qout hyperuricaemia, pneumonia, kidney damage, Lesch-Nyhan

syndrome and cardiovascular diseases.[1] Hence, estimation of the level of UA in human blood or urine indicates early observe for the presence of these disorders. In recent times, numerous techniques developed determination of UA has been reported, such as enzymatic method, [2] electroanalysis,[3] high performance liquid chromatographys, [4] spectrophotometry, [5] flourimetry[6] and chemiluminescence. [7] In which, the electrochemical determination of UA has concerned a lot of attention in recent years due to its simplicity, quick detection and high selectivity. Earlier used the electrochemical procedures were based on the oxidation of UA at the pre-treated carbon electrode and polymer modified electrode. [8]

In recent years, the use of metal nanoparticles as analytical and bio analytical sensors has been receiving major attention because of their abnormal optical, electronic, and chemical properties. [9-11] Large number of methods has been developed for the fabrication of metal nanoparticles. However, the major disadvantages of the familiar methods include use of external reducing chemicals, poor control, over nanoparticle size distribution, and the poor diffusion of the nanoparticles in the polymer mass. [12]

PANI possesses a excellent properties such as highly tuneable conductivity, easy fabrication process and environmental stability in both of its doped (conducting) and dedoped (insulating) forms. [13] Furthermore, it is an interesting material for a sensor and biosensor interfaces as it can act as an effective mediator for electron transfer of redox reactions and suitable for covalent binding of bio molecules due to the presence of active functional groups. [14]

More recently, the interest in PANI based material interlaced with bio molecules for use as platforms to electrochemical sensors and biosensor has increased. It is believed that the use of conducting polymers may provide a large stability to the immobilized biomolcule in the PANI composite, potential enhancing the analytical capability.[15] The search for

biopolymers for developing electrochemical sensors and biosensors aims to replace synthetic materials, complying with sustainability procedure.[16] In the direction, the development of material using naturally-derived biomolecules and biopolymers, whose versatility, biodegradability, and non-toxicity can confer advantages over synthetic materials is an area of current intense research.[17]

In few literature reported that the biopolymers extracted from the red seaweeds and layer-by-layer film prepared with polyaniline for electrochemical detection of chromium.[18] The specific capacitance of polyaniline was improve the blend with biopolymer of carboxymethyl cellulose with aniline during the polymerization.[19] Several other biopolymers blended with polyaniline to nanostructure morphological materials and used in various applications. [20-22]

Brown seaweeds are the second most abundant group of algae comprising of 2000 species. It is the outstanding source of bioactive compounds such as carotenoids, dietary fibre, protein, lipids, polysaccharides, polyphenols, essential fatty acids, vitamins and minerals. [23,24] The major structural polysaccharides of brown seaweeds are alginate. Alginate is the salt of alginic acid, a linear copolymer of D-mannuronic acid and L-guluronic acid (1-4)-linked residues, arranged in heteropolymeric or homopolymeric blocks.[25,26] Macro algae of seaweed also have the sum of bioactive compounds such as amino, sulphate, carboxyl and hydroxyl groups. [27]

In this work, we have investigated seaweed bio polymers incorporated into conducting PANI through one-step chemical oxidation method. The characteristics and electrochemical properties of the synthesized samples were investigated by FTIR, UV–vis, XRD, HR-SEM, EDAX, TG/DTA and N_2 adsorption/desorption test as well as electrochemical measurements. The cyclic voltammetry (CV) and difference pulse (DPV)

voltammetry was employed to construct an enhanced sensing platform for the electrochemical detection of uric acid (UA).

2. Experimental

2.1. Materials

Brown seaweed of *Padina tetrastromatica* was collected from Mandapam, Rameswaram, East Coast of India. The collected seaweed was cleaned well with sea water to remove all the extraneous matter and then washed thoroughly using double distilled water. Then it was shade dried, ground to powder and stored in air tight container for further studies. Aniline ($C_6H_5NH_2$) and ammonium persulfate $(NH_4)_2S_2O_8$ (APS) were purchased from Merck specialties, India. Aniline was distilled prior to use. All supplementary chemicals such as sodium hydroxide, hydrochloric acid and methanol were of analytical grade and used without further purification. Deionised water was used throughout all the experiment.

2.2. Preparation of seaweed extract (SE)

Dried and powdered seaweed samples (0.5 g) were suspended in 50 ml of methanol and vigorous stirring for 30 min and then kept for 24 h extraction at room temperature. To this solution was sonicated for 30 min and filtered through a whatman 41 filter paper. The filtrates were labelled as methanol extract, 50 ml of deionised water was added to the remaining seaweed residue sonicated for 30 minutes, and filtered; this filtrate was labelled as aqueous extract. Finally, both (methanol and aqueous) extracts were mixed and methanol solvent was evaporated to dryness under pressure using a rotary evaporator to dryness under pressure using a rotary evaporator (Superfit Rotavap, model DBV-7D) to get a dark green colour semi-solid residue. The product thus obtained was designated as the SE and used for further experiments.

2.3. Preparation of seaweed-polyaniline (SE-PANI) nanofibre

About 0.2 g of methanol free seaweed extract was dissolved in 50 ml of HCl (0.5 M) at room temperature. 0.2 M of aniline monomer was introduced the above solution and then mixture was sonicated for 30 min to facilitate the adsorption of aniline into the seaweed extracts. 20 ml of 0.5 M APS was added into the above system at 0-5°C ice bath for 4 h with continuous stirring. The resulting mixture was settled for 24 h to complete chemical reaction followed by washed more times with deionised water until filtrate was colourless, and then dried at 60°C for hot air oven to obtain 1.062 g of dark green powder, which is designated as SE-PANI.

2.4.Characterization

The structural characterizations of the samples were prevailed through Fourier transforms infrared (FT-IR, SHIMADZU, using KBr pellets) spectroscopy in the range of 400-4000 cm^{-1}. UV-Vis spectrophotometer (UV-vis, SHIMADZU, UV-2401pc) was used to observe the optical properties of the nanofibre. X-ray diffraction (XRD) studies were carried out in 2θ range of 10–80° using X-ray diffractometer ((X'Pert PRO diffractometer) of Cu Kα radiation (λ = 0.15406 nm) with the scanning rate of 0.01^{o}/step with 2θ ranging from 10° to 80^{o}.). The XRD patterns were analyzed by matching the observed peaks at the standard pattern. The morphology of the resulting products was observed by high resolution scanning electron microscope (FEI QUANTA FEG-250 HR-SEM and Energy dispersive X-ray photoelectron spectroscopy (EDAX). Thermo gravimetric analysis was carried on (SII EXSTAR6200 TG/DTA) in a nitrogen atmosphere upto 1000°C at a heating rate of 10°C/min using aluminium pan as a reference. Nitrogen adsorption–desorption isotherms were performed with an ASAP 2020 Micromeritics analyzer at 77 K, and the specific surface areas (SBET) was determined by Brunauer–Emmett–Teller (BET) method. The pore size

distribution was calculated according to the Berrett–Joyner– Halenda (BJH) method. Electrochemical behavior and bio-sensing property of the nanofibre were studied using cyclic voltammetry (CV) and difference pulse voltammetry (DPV) in (AUTOLAB CHI1102A) electrochemical workstation with a conventional three-electrode electrochemical cell using a glassy carbon (GC) electrode (3 mm diameter), an Ag/AgCl (sat. KCl) and a Pt wire as the working, reference, and counter electrodes, respectively.

3. Results and discussion

3.1. FT-IR Analysis

The FT-IR spectrum of SE, PANI and SE-PANI nanofibre are shown in Fig. 1A. The main characteristics peaks of SE (curve a) at 3409 cm^{-1} and 2921 cm^{-1} are assigned to the stretching vibrations of O–H and C–H bonds, respectively. The strong bonds at 1629 cm^{-1}, 1422 cm^{-1} and 1034 are caused by the stretching of $–COO^-$ (asymmetric), $–COO^-$ (symmetric), and C-O-C respectively. The band at 1116 cm^{-1} is attributed to the bending vibration of C-H bond. The peaks at 670 and 601 cm^{-1} were attributed to the asymmetric and symmetric O=S=O deformation of sulphates.[28-31]

The main characteristic IR peaks of PANI (curve b) were observed at 1567 cm^{-1} and 1481 cm^{-1} ascribed to the C=C stretching deformation of quinoid and benzene rings, respectively, 1297 cm^{-1} and 1243 cm^{-1} to the C-N and C=N stretching band of an aromatic amine and 1113 cm^{-1} and 799 cm^{-1} to the plane and out of plane bending of C-H, respectively.[32-33]

However, there are several differences between the FTIR spectrum of the SE-PANI in the SE and the spectrum of PANI (curve c) is found near 3402 and 3227 cm^{-1}. This signal is broad and strong in the SE-PANI yet very weak in the polyaniline spectrum

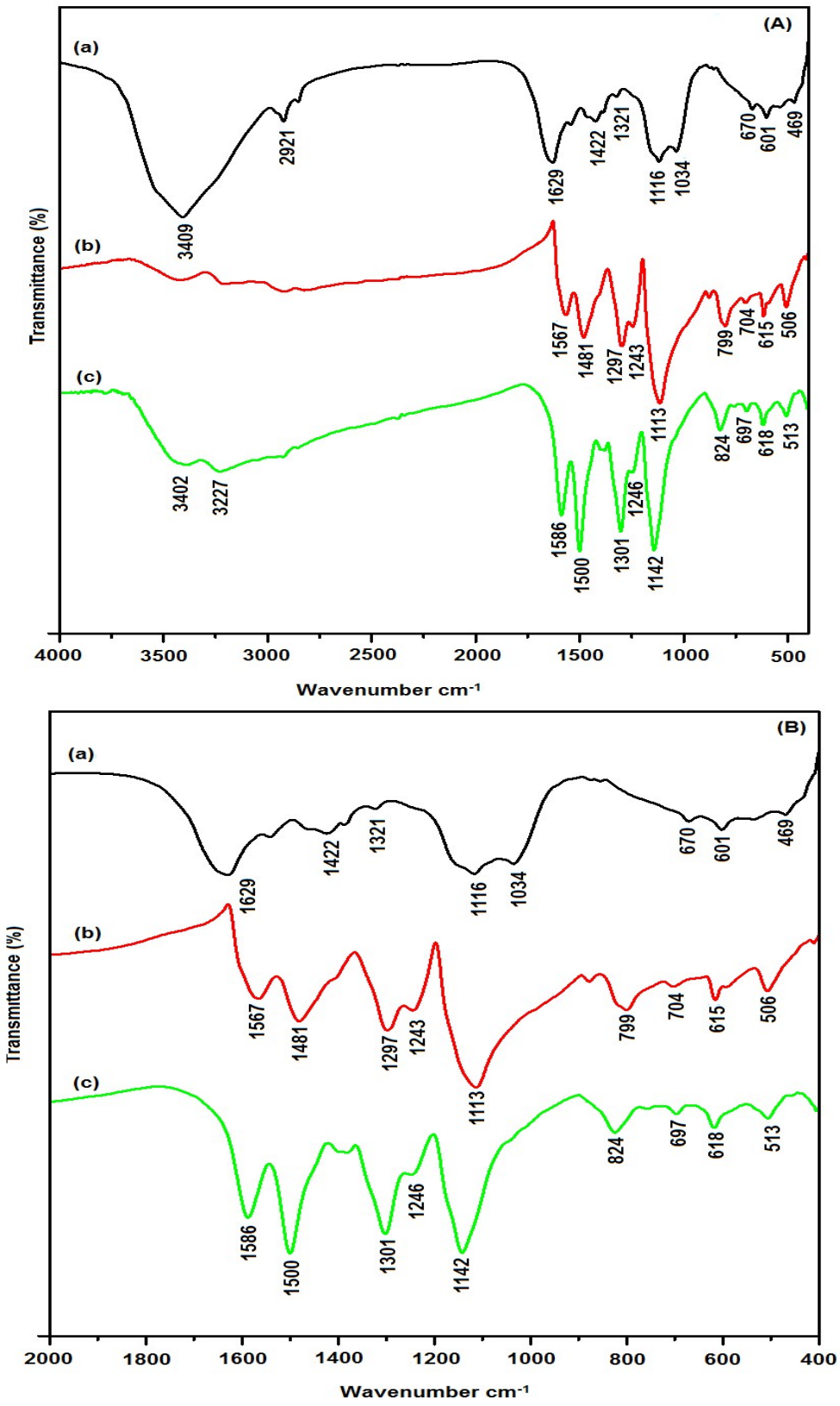

Fig. 1. FT-IR spectra of (a) SE (b) PANI and (c) SE-PANI.

To rule out moisture effects, spectra from identical samples saturated with water were compared as a function of time and drying. Water was completely removed under the drying conditions used for the samples. The evidence suggests that SE exists in the SE-PANI nanofibre. The spectra confirmed that the carboxylate groups of SE were dissociated to COO- groups which complexed with protonated amino groups from SE-PANI through electrostatic interaction. The interaction may result in SE functioning as a chemical dopant for PANI.

Moreover, as the SE-PANI nanofibre formation proceeded, O-H bonding would also be expected because of an increase in intermolecular interaction such as hydrogen bonding between SE and PANI.[34]Then also shift some peaks and changes of relative intensity in presence of SE in PANI. In particular, the peaks at 1567, 1481, 1297, 1243, 1113 and 799 cm^{-1} that shifted to higher wave number of 1586, 1500, 1301, 1246, 1142 and 824 cm^{-1} respectively shown in the enlarge (wavenumber between range in 2000-400 cm^{-1}) the Fig. 1B at finger print regions. These results are further confirmed that the SE was successfully blended on the PANI matrix.

3.2. X-Ray Diffraction Analysis

The XRD patterns of SE, PANI and SE-PANI nanofibre are displayed in Fig. 2 (a-c). The diffraction pattern of SE shows typical two sharp peaks at $2\theta = 29.46^{\circ}$ and 31.71° which is indexed to the plane of (220) and (221) respectively. These obtained values clearly indicate the semicrystaline nature of SE. Broad peaks appeared at $2\theta = 15.23$, 20.51, and 25.39° corresponding to (011), (020) and (200) planes (curve b) indicate that as prepared PANI is in emeraldine salt form.[35] As for SE-PANI sample, along with all the diffraction peaks corresponding to the characteristic diffraction peaks of individual SE and PANI samples, some new peaks are appeared at $2\theta = 22.90^{\circ}$, 28.54° and 34.11° which are corresponding to the plane of (210), (211) and (310) respectively. It is obvious that the crystallinities of SE-PANI

nanofibre increased with the introduction of SE, due to the enhancement of intermolecular interaction. [36]

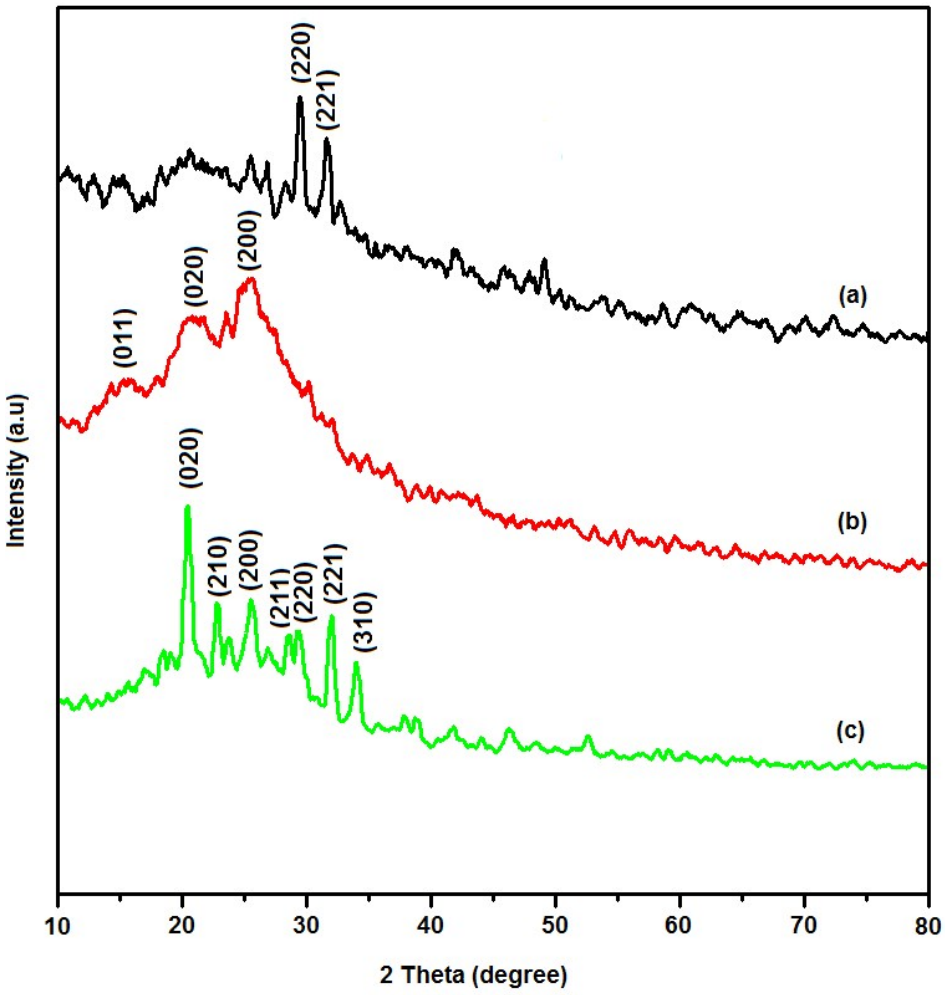

Fig. 2. XRD patterns of (a) SE (b) PANI and (c) SE-PANI.

3.3. UV-Visible Spectroscopy

UV-Vis absorption spectroscopy is a powerful tool to characterize the interfacial interaction between SE and PANI. The UV-Vis absorption spectra of the SE, PANI and SE-PANI nanofibre are shown in Fig. 3(a-c).

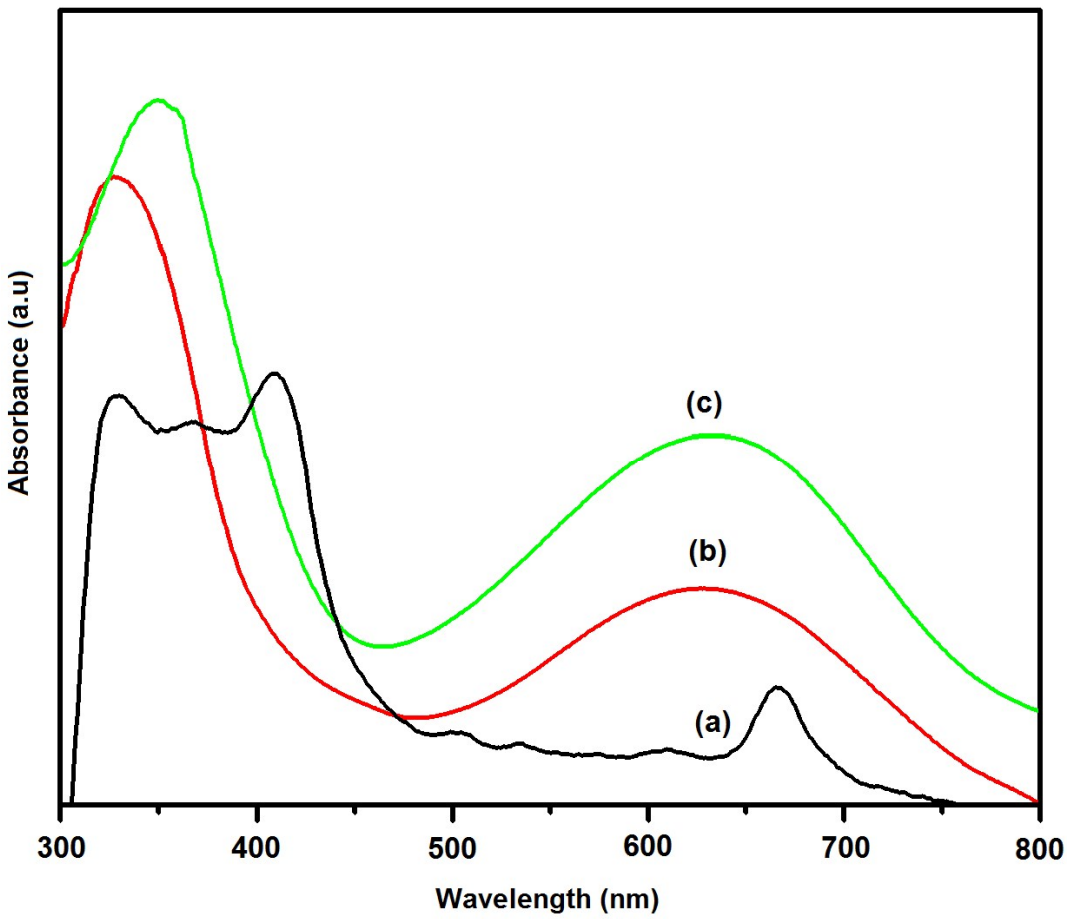

Fig. 3. UV-Vis spectra of (a) SE (b) PANI and (c) SE-PANI

The absorption spectrum of the SE exhibits three absorption peaks at 328, 408 and 667 nm which is the characteristic of SE extract. The spectrum for PANI and SE-PANI nanofibre (curve b-c) shows two absorption bands at around 326 and broad band at 633 nm. The first absorption band arises from π-π* electron transition within benzenoid segments, whereas second absorption bands are related to doping level and formation of conducting polarons (quinoid segments), respectively.[37,38] On comparison to pristine PANI, the absorption bands at 326 and 633 nm have been red shifted to 347 and 643 nm respectively in SE-PANI might due to the successful interface of SE and PANI with the polymer matrix

3.4. Morphological and Elemental Analysis

Surface morphology of the SE, PANI and SE-PANI nanofibre are shown in Fig. 4(a-c). The SEM images of SE exhibit of aggregation of several smaller interconnected fiber-like structures. Further, it is observed that seaweed surfaces are well covered and regular shaped cellulosic fibres were present in the cell wall component of the seaweed.

In Fig. 4b the aggregated morphology was obtained for the pristine PANI, where as SE-PANI nanofibre show the fibrillar network like morphology structure was formed after the addition of SE into the monomer solution, which biopolymer-monomer complexes former by electrostatic interaction between carboxylic groups of SE and amino groups of aniline monomer. [39] From the morphology study, the comparison between pristine PANI and SE-PANI nanofibre image (Fig. 4c) is clear that, SE is an important template material in the formation of nanostructure of polyaniline matrix, and such as nanofibre with a porous network is favourable in electrochemical applications

The elemental composition of the seaweed extract analyzed by EDAX spectrum shown in Fig. 4(d-f), indicates that, the seaweed sample was composed of C, O, Na, Al, S, Si, Cl, K, Ca and Fe elements, hence confirming the SE has a various element presented as polysaccharide. These most elements also presented in SE-PANI nanofibre, clearly indicate that the seaweed is present in the PANI matrix.

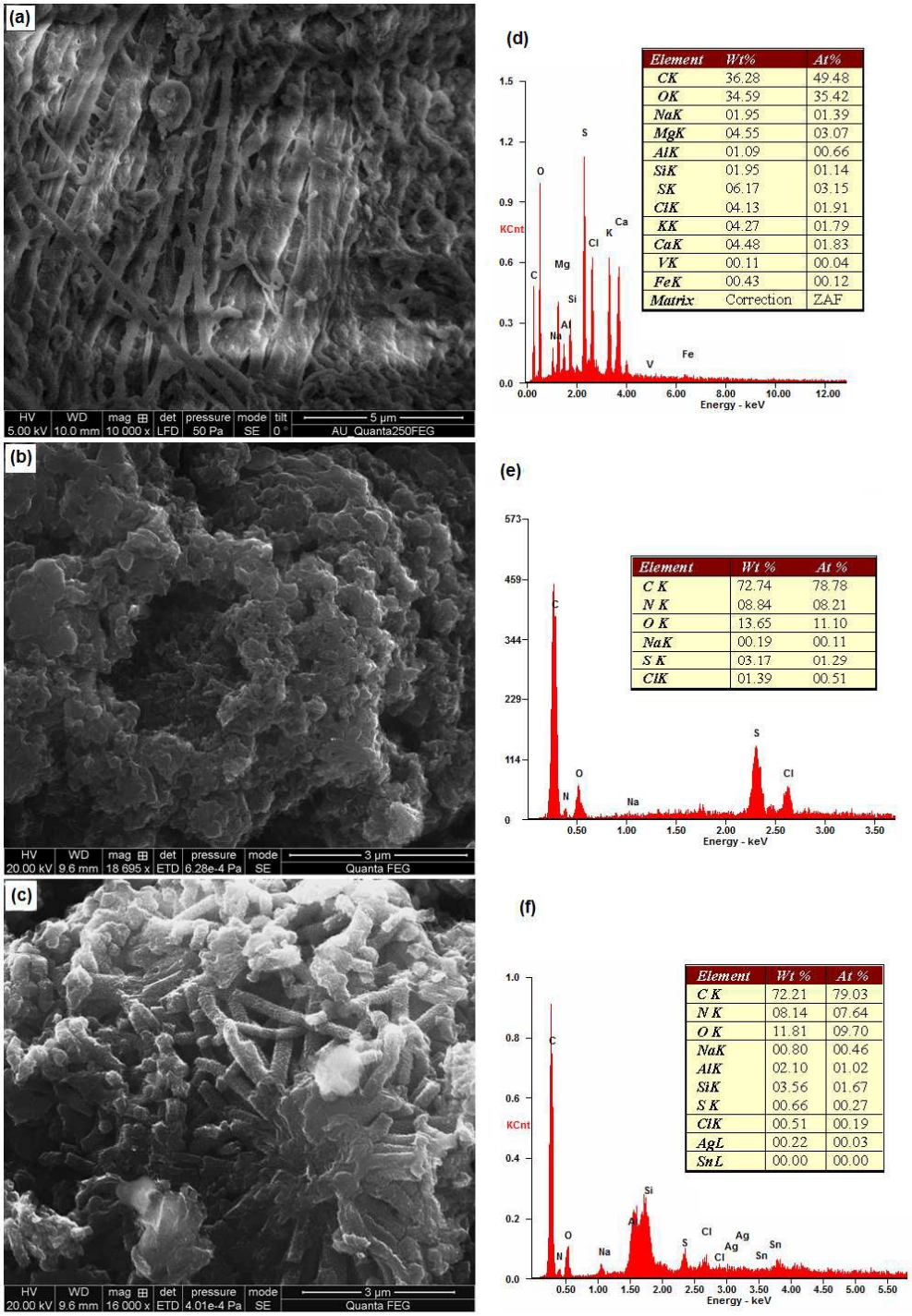

Fig. 4. HR-SEM images of (a) SE (b) PANI and (c) SE-PANI; Elemental analysis of (d) SE (e) PANI and (f) SE-PANI.

3.5 BET Analysis

The porous distinctive SE-PANI nanofibre was further characterized by BET analysis, the nitrogen adsorption/desorption isotherms and BJH pore size distribution curves (inset) and shown in Fig. 5. According to the IUPAC classification, the isotherms are type IV with H3 hysteresis loop at a height relative pressures on (P/P_0 =0.9509) are the typical characteristics of mesoporous materials. [40]

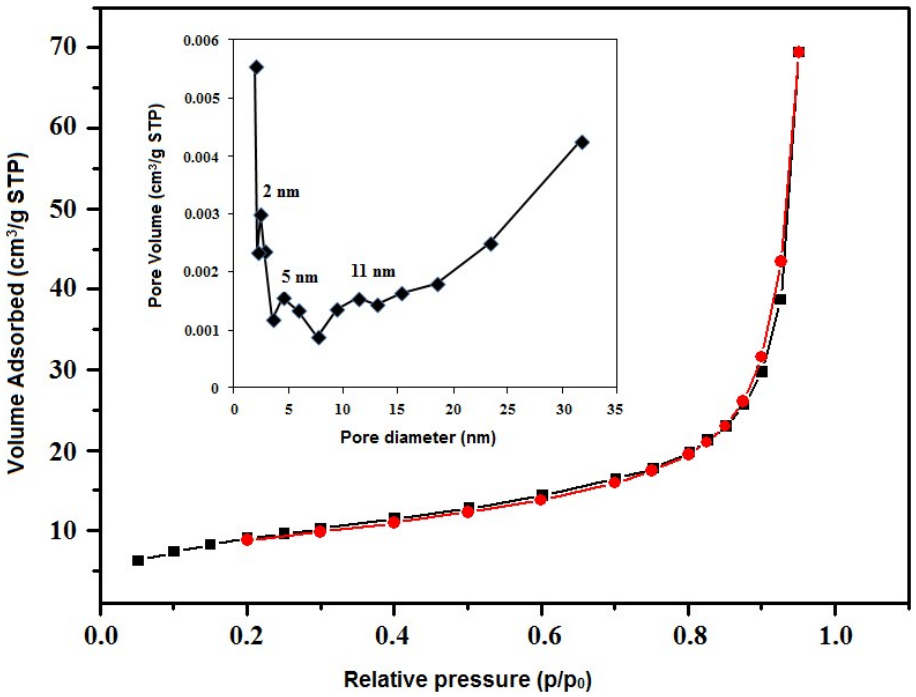

Fig. 5. Nitrogen adsorption-desorption isotherms and inset the pore size distribution curve of SE-PANI nanofibre.

The specific surface area calculated by the BET equation is 36.47 m^2/g, the pore volume distribution determined by the BJH method was found to be 0.1073 cm^3g and the average radius of pores is 15.79 nm (Table 1), which indicates that the SE-PANI nanofibre is a mesoporous structure.

Table 1. List of textural parameters of SE, PANI and SE-PANI nanofibre.

Samples	Surface area (m^2/g)	Pore volume (cm^3/g)	Average pore diameter (nm)
SE	0.42	0.0017	16.65
PANI	33.87	0.0613	7.24
SE-PANI nanofibre	36.47	0.1073	15.79

However, the multimodal pore structure of SE-PANI can be clearly observed from the pore size distribution curve (inset in Fig. 5). The pore size distribution curves shows that the diameter for the SE-PANI nanofibre is mainly centered at 2-5 nm and 11-30 nm, respectively. Based on the SEM image (Fig. 4c), the formation of porosity in the SE-PANI nanofibre is due to the inter-agglomeration of seaweed with polyaniline. SE-PANI nanofibre having porous structure with high BET surface areas possibility may have to excellent electrochemical properties of these materials where as easy to able move the electrons and ions. [41-43]

3.6. Thermal Properties

Seaweed offers numerous advantages, such as excellent heat insulation, heat capacity and brilliant flame retardant characteristics. [44] Thermo gravimetric analysis (TGA) provides quantitative determination of the degradation of a nanofibre and differential thermo gravimetric (DTG) curve peak location provides a mutual effect of the nanofibre components on the thermal properties. The TG and DTG curves of SE, PANI and SE-PANI nanofibre are shown in Fig. 6a and 6b respectively. As show in TG curve of SE and PANI samples, 16% and 14% of weight loss was occurring before 130°C is due to the removal of water, while SE-

PANI sample show only 4% loss before 100°C indicating that the absorbed water in the SE-PANI nanofibre is less than that of SE and PANI.

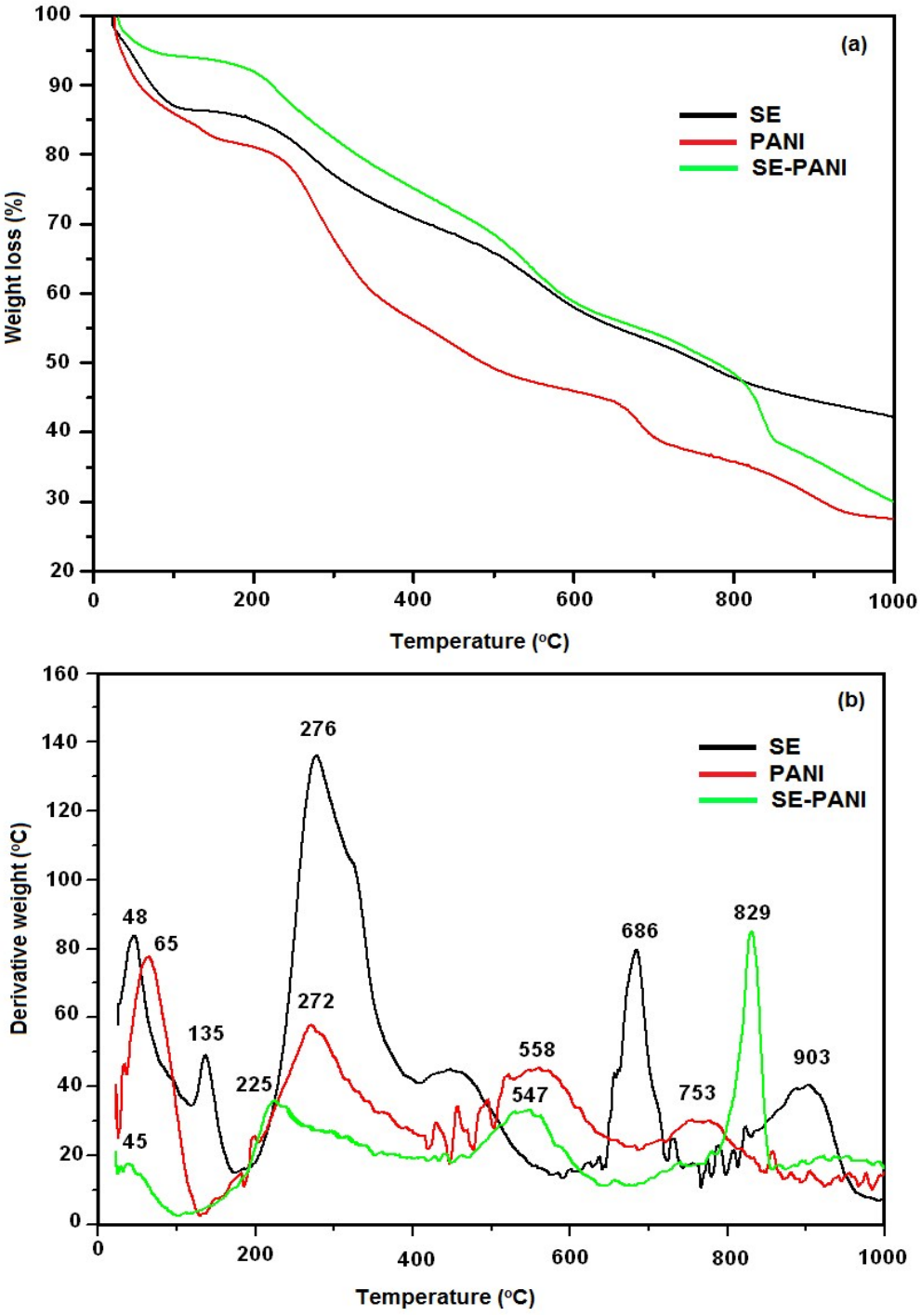

Fig. 6. (a) TGA and (b) DTG curves of SE, PANI and SE-PANI nanofibre.

Decomposition of seaweed polysaccharide molecules were observed in three steps. As illustrated by the DTG curve in Fig. 6b, the first step is more rapid and the major decomposition was observed in the range of 200-600ºC with a peak maximum at 276ºC which is in close agreement with the reported value of ethanol treated *Enteromorpha crinite* seaweed.[45] The other two additional decomposition peaks were observed at higher temperature (683 and 903ºC). However, the PANI and SE-PANI samples were decomposed constantly in the temperature range of 200 to 800ºC ascribed to decomposition of polyaniline chains.[46]

As a result of the examination of the thermal properties, SE-PANI nanofibre showed higher thermal stability up to 800°C than that of SE and PANI. This could be explained on the basis of the anionic nature of sulphate ions present in the SE which may be incorporated into parts of the molecular complex of the PANI chains and formation of hydrogen bond between carboxylic acid and nitrogen thereby increase in the thermal stability of the SE-PANI nanofibre.[47] Further heating to 1000°C the SE, PANI and SE-PANI nanofibre left a residue of 42, 28 and 30 % respectively.

3.7. Electrochemical Properties of SE-PANI/GCE Modified Electrode

The electrochemical characteristics of pristine PANI and SE-PANI nanofibre were analyzed using cyclic voltammetry (CV) and electrochemical impedance spectroscopy (EIS). The CV was carried out with a potential range of -0.2 to 1.0 V in absence of oxygen and 0.5M of H_2SO_4 was used as an electrolyte solution. The PANI or SE-PANI modified glassy carbon electrode was used as a working electrode, platinum and Ag/AgCl was used as a counter and reference electrode respectively. The working electrodes for evaluating the electrochemical performance of as-prepared samples were fabricated by casting 5 μL^{-1} of the synthesized samples suspension on the electrode surface, and dried for 30 min at room

temperature. The suspension can be obtained with 5 mg of SE-PANI synthesized material was dispersed in 5 ml of N-methyl-2-pyrrolidone (NMP). [48,49]

To evaluate the electrochemical characteristics of the sample, CV curves in 0.5 M H_2SO_4 electrolyte at scan rate of 100 mV s^{-1} were performed at the potential window from -0.2 to 0.8 V versus SCE. As shown in Fig. 7a, the shapes of the CV curve of PANI and SE-PANI distinct from that of SE. The contribution of pure SE to the capacitance is very small and can be neglected.

There are three pairs of redox peaks are found on the CV curves of the pure PANI and the SE-PANI nanofibre, respectively. The first couple of peaks are caused by the redox transition of PANI between the leucoemeraldine form and polaronic emeraldin form. The second couple of peaks are due to the transformation of the p- enzoquinone/hydroquinone couple. The third couple of peaks are ascribed to the formation/reduction of bipolaronic pernigraniline and protonated quinonediimine.[50,51] Electrochemical capacitance is proportional to their CV curve area. Apparently, the CV curve area of SE-PANI is larger than that of the parallel sample of pure PANI.

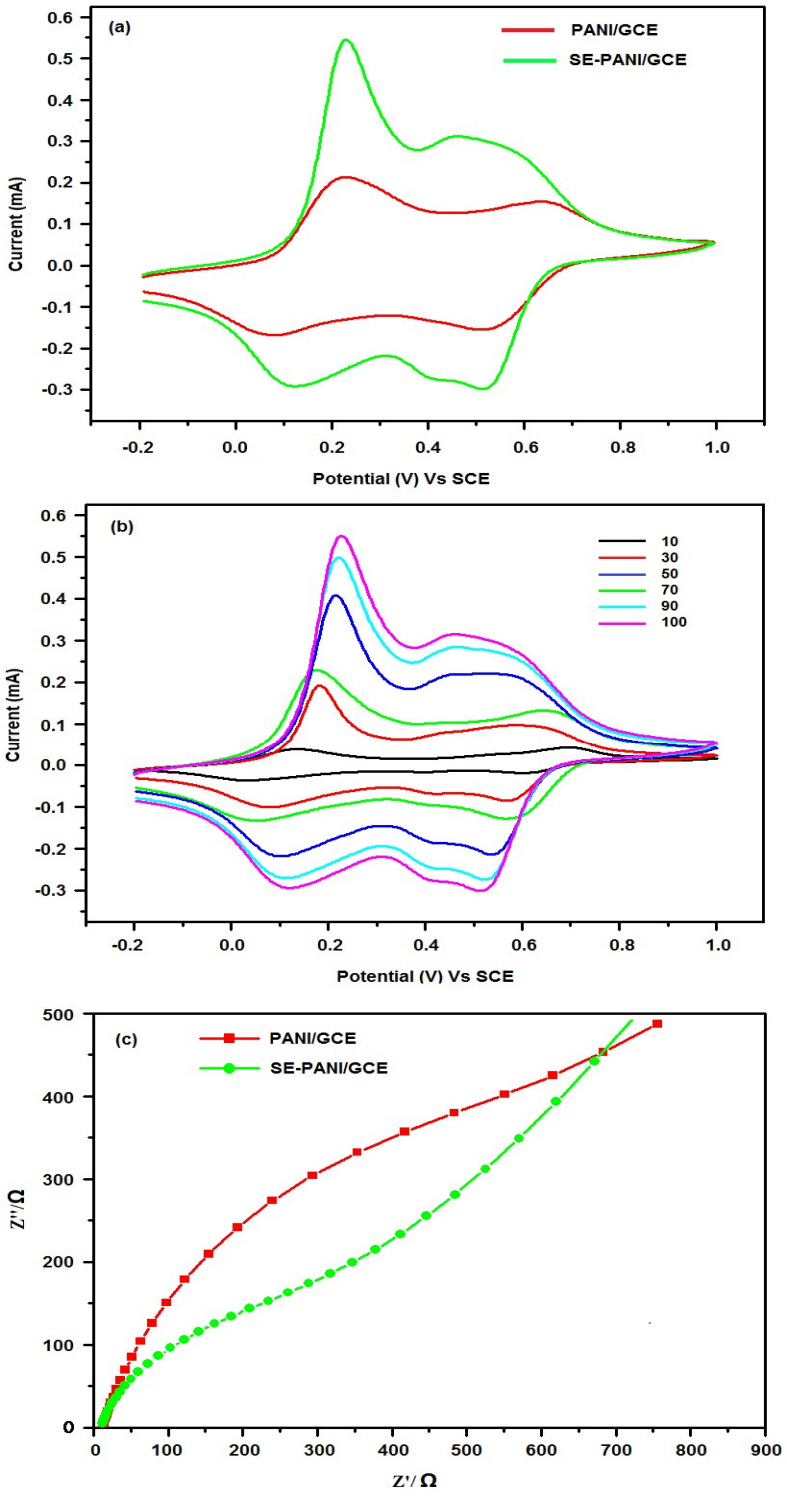

Fig. 7. (a) CV of PANI/GCE and SE-PANI/GCE at a scan rate of 100 mVs^{-1} in 0.5 M H_2SO_4. (b) SE-PANI/GCE at different scan rates. (c) EIS obtained for PANI/GCE and SE-PANI/GCE.

The Brunauer-Emmett-Teller (BET) measurement indicates that the specific surface area of SE-PANI (36.47 m^2/g) is larger than pure PANI (33.87 m^2/g), which is favorable for ion transportation and, hence, provides larger capacitance. As indicated in Fig. 7a, in comparison to pure PANI, the regular nanostructured network of SE-PANI enhances the surface area for redox reactions and shortens the distance for electrolyte ions transport, thereby leading to a high special capacitance.

The relationship between peak currents and scan rates has been investigated at SE-PANI electrode (Fig. 7b). As show in Fig. 7b, the redox currents of the SE-PANI modified electrode increases with the increase in scan rates (10, 30, 50, 70, 90 and 100 mVs^{-1}), indicating its good scan rate ability of the electrode. The increase of scan rates and shifting of oxidation peaks were due to the resistance of modified electrode.

The enhanced the electrochemical performance of SE-PANI nanofibre modified electrode is further confirmed by EIS and the resulting Nyquist plots are shown in Fig.7c. The estimated charge transfers resistance (R_{ct}) values were found to be 612.6 Ω, and 348.4 Ω for pristine PANI and SE-PANI nanofibre modified GC electrode, respectively. The smaller Rct suggests a faster faradic reaction with much lower resistance. The decreased Rct of SE-PANI electrode may be attributed to the combined effect of PANI and SE, in which the structure can facilitate the efficient access of electrolyte ions to the electrode surface and shorten the ion diffusion path. Thus SE-PANI nanofibre indicates higher conductivity and controlled electron diffusion process. [52]

3.8. Electrochemical Behaviour of Uric acid on SE-PANI/GCE Modified Electrode

Electrocatalytic activity of uric acid (UA) was investigated with different electrodes by cyclic voltammograms shown in Fig. 8. The voltammetric responses to 1.0 mM UA were measured for three electrodes: bare GCE, PANI/GCE and SE-PANI/GCE with the potential range of −0.2 to 0.8 V in 0.1 M phosphate buffer (pH 7.0) at scant rate of 50 $mVs^{-1.}$

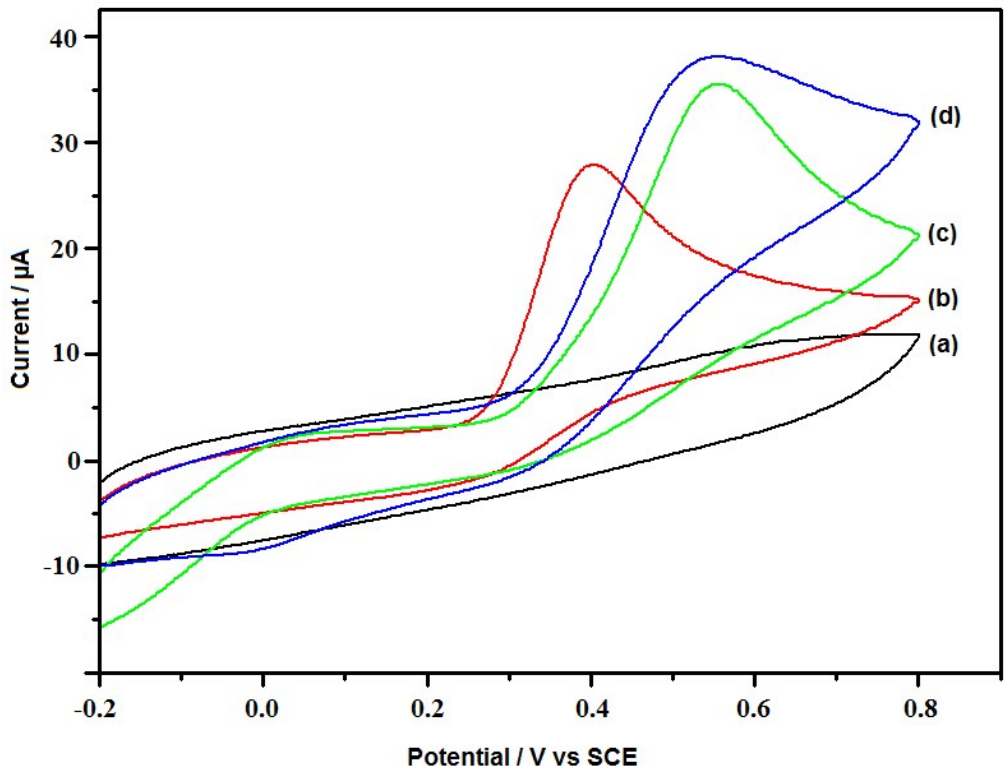

Fig. 8. CVs of (a) bare GCE in 0.1 M PBS (pH 7.0), (b) bare GCE, (c) PANI/GCE and SE-PANI/GCE in 0.1 M PBS (pH 7.0) solution containing 1.0 mM uric acid at scan rate 50 mVs^{-1}.

There are no apparent anodic peaks observed in the blank deaerated 0.1 M phosphate buffer PBS on the bare electrode (Curve a). A low current and broad anodic peak appears at the bare GCE electrode for PBS with 1.0 mM UA at approximately 0.41 V and peak current of 27.8 µA measured (Curve b), suggesting slow electron transfer kinetics, which were presumably due to the fouling of the electrode surface by the oxidation product. It was reported that the oxidation of UA was irreversible at glassy carbon and metal electrodes.[53]

In contrast, on the PANI/GCE (curve c), the anodic peak currents are significantly increased from peak potentials of GCE as 0.56 V. However, a sharp well-defined anodic peak appears for the SE-PANI/GCE electrode (Curve d). The oxidation peak current is 39.28 µA

which is found to be enhanced greatly and peak potential also shifts negatively to 0.53 V. These phenomena suggested that the oxidation of UA is more favorable at the SE-PANI/GCE electrode.

3.8.1. Effect of Scan rate and pH

The effect of scan rates for the oxidation peak current of UA at the SE-PANI/GCE was studied (Fig. 9) at different scan rates (10–100 mV s^{-1}). The scan rates and the oxidation peak current increased linearly with slight shift in the oxidation peaks potential.

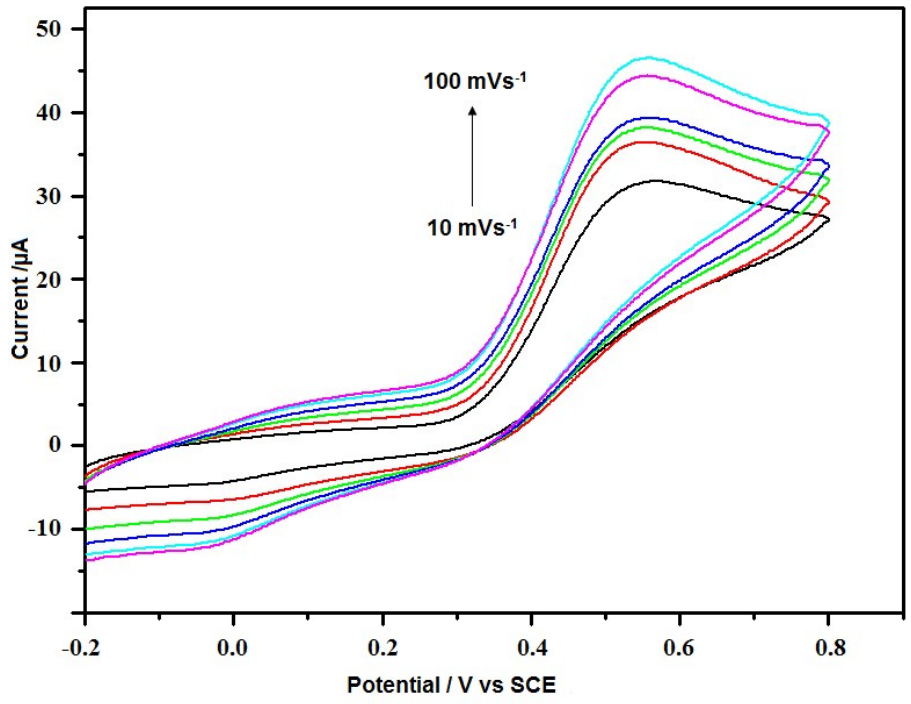

Fig. 9. CVs of 1.0 mM UA on SE-PANI/GCE at different scan rates (10, 30, 50, 70, 90 and 100 mVs^{-1}) 0.1 M PBS (pH 7.0).

The peak potentials shifted slightly toward the positive to the negative direction at higher scan rates, suggesting that UA oxidation processes of the nanofibre electrode were surface-confined electrochemical processes not diffusion controlled electrochemical process.

The effect of pH to the electrocatalytic oxidation of UA at the SE-PANI/GCE was investigated with different pH (4 to 9) buffer solutions containing 1.0 mM UA using a cyclic voltammetry as shown in Fig. 10

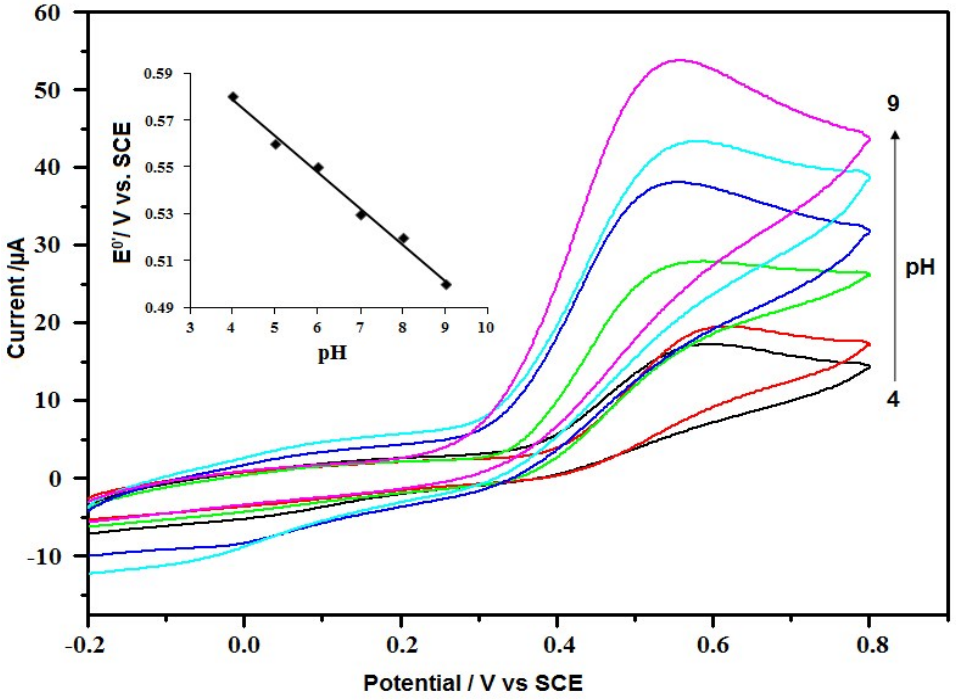

3.

Fig. 10. CVs of 1.0 mM UA on SE-PANI/GCE in 0.1 M PBS with pH values of 4.0, 5.0, 6.0, 7.0, 8.0 and 9.0. Inset, the plot formal potential vs. pH value. Scan rate: 50 mVs^{-1}.

The peak current for the electrocatalytic oxidation of UA in base solutions was higher than that of in acid solution, which is due to the instability of UA in acid solution. The anodic peak potential (E_{pa}) for UA shifts to more negative values as increase in pH and a good linear variation was observed as illustrated with inset in the Fig. 10. This indicates that SE-PANI nanofibre modified electrode has high catalytic activity, in the neutral and alkaline media. [54] Hence, the detection of UA with pH 7.0 was chosen as optimum other experiments.

8.2. Determination of Uric acid

As shown in Fig. 11 the difference pulse voltammetry (DPV) obtained for UA in concentration range of 5×10^{-5} to 5×10^{-3} M at the SE-PANI/GCE modified an electrode in 0.1 M PBS (pH 7.0). The oxidation current of uric acid increased with the increase in uric acid concentration (each step with increment of 50 µM) as shows in Fig. 11.

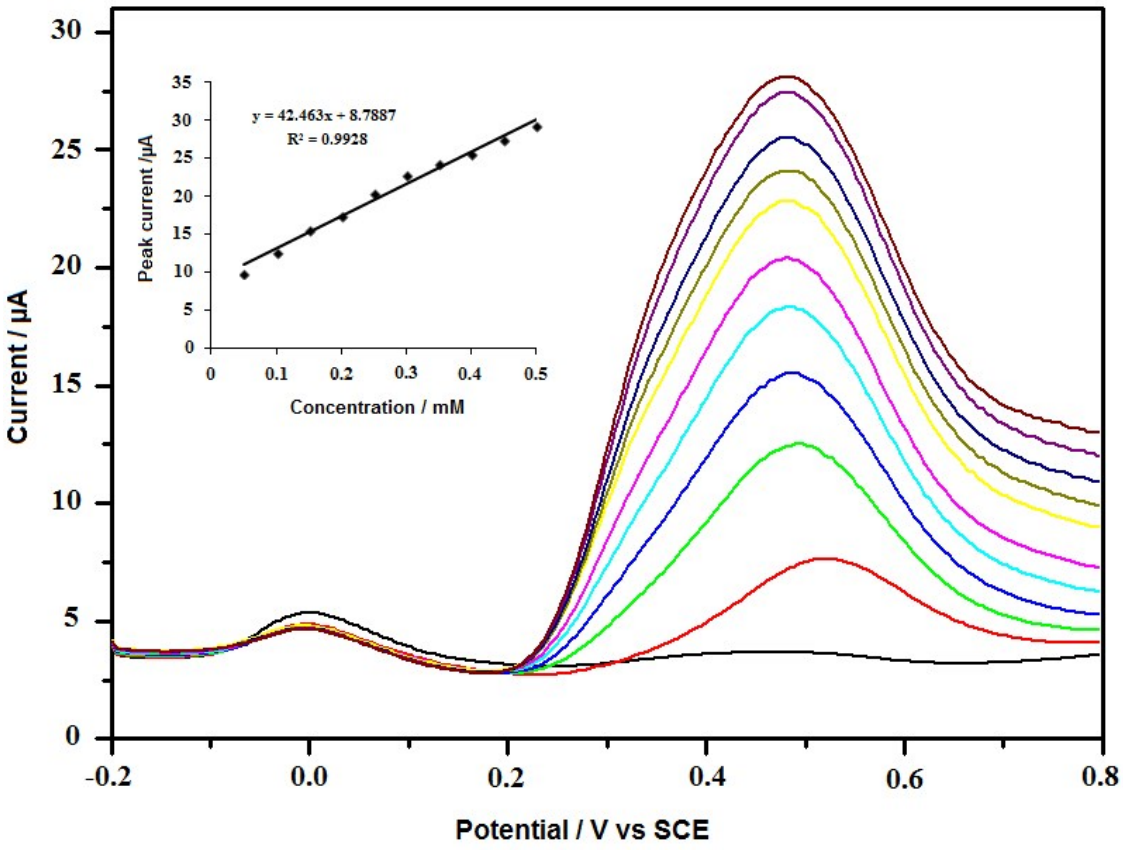

Fig. 11. DPVs of SE-PANI/GCE in 0.1 M PBS (pH 7.0) containing different concentration of UA from (a) to (k) are 0, 50, 100, 150, 200, 250, 300, 350, 400, 450 and 500 µM scan rate at 50 mVs^{-1}. Inset, the plot of peak current vs UA concentration.

The calibration plot of UA concentration vs peak currents is present in the inset of Fig. 11. The increasing in concentration of UA increases peak currents and obtain the

correlation coefficient 0.9976. The reproducibility of the experiment was repeated with three times and obtained the satisfactory results in the above concentration ranges. In addition, the detection limit was estimated to be 0.104×10^{-6} M L^{-1} at a signal to noise ratio of 3, which is calculated using 3sB/S, where sB is the standard deviation obtained from 10 blank measurements, and S is the sensitivity of the measurement (slope of the calibration curve).[55]

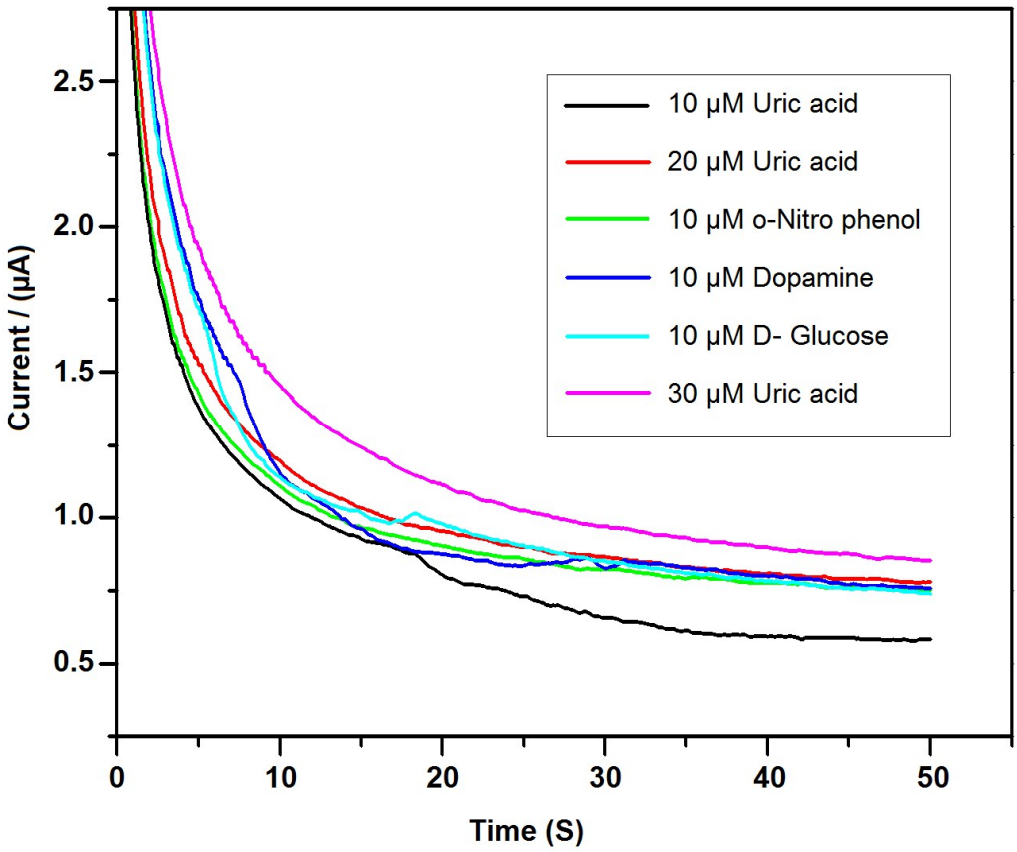

Fig. 12. Effect of interfering study on uric acid response.

To evaluate the selectivity of biosensor, the major interfering compounds such as o-nitrophenol, dopamine and D-glucose are taken. During sensing about 10 μM of each compound was added and the investigation was carried out to evaluate interference. Fig. 12 show the amperogram obtained and it confirms no significant changes by the interference. [56]

The uric acid detection limit was measured at pH 7 with various modified electrodes reported on the literature are shown in Table 2. From the table values, it is noted that SE-PANI nanofibre shows lowest detection limit for UA determination at physiological pH.

Table 2. Comparison of uric acid detection limit with various modified electrodes at pH 7.0.

Electrode	pH	Linear Range (M)	Detection limit (μM)	References
E-HA/GCE	7.0	1.0×10^{-7} to 3.0×10^{-5}	0.142	[57]
Graphene/CFE	7.0	1.9×10^{-7} to 4.9×10^{-5}	0.132	[58]
Au/RGO/GCE	7.0	8.8×10^{-6} to 5.3×10^{-5}	1.80	[59]
Trp-GR/GCE	7.0	1.0×10^{-5} to 1.0×10^{-3}	1.24	[60]
SE-PANI/GCE	7.0	5.0×10^{-5} to 5.0×10^{-3}	0.104	In this work

3.8.3. Simultaneous Determination of UA and AA

The presence of the SE-PAN nanofibre at GCE surface can resolve the overlapped voltammetric response from two well-defined oxidation peaks at 0.28 and 0.47 V in CV (Fig. 13) and 0.19 and 0.42 V in DPV (inset of Fig. 12) corresponding to the oxidation of AA and UA, respectively. The separations between the two peak potential were 0.23 V, which was large enough for the selectively and simultaneous determination of UA and AA in their binary mixture. Thus, experiment with interferences including AA and UA was performed to test the selectivity of the SE-PANI/GCE sensing platform. As show in Fig. 13 (inset), UA exhibits well-defined DPV wave with good separations from AA. Therefore, the selective detection of UA in the presence of AA is possible by SE-PANI nanofibre modified GCE.

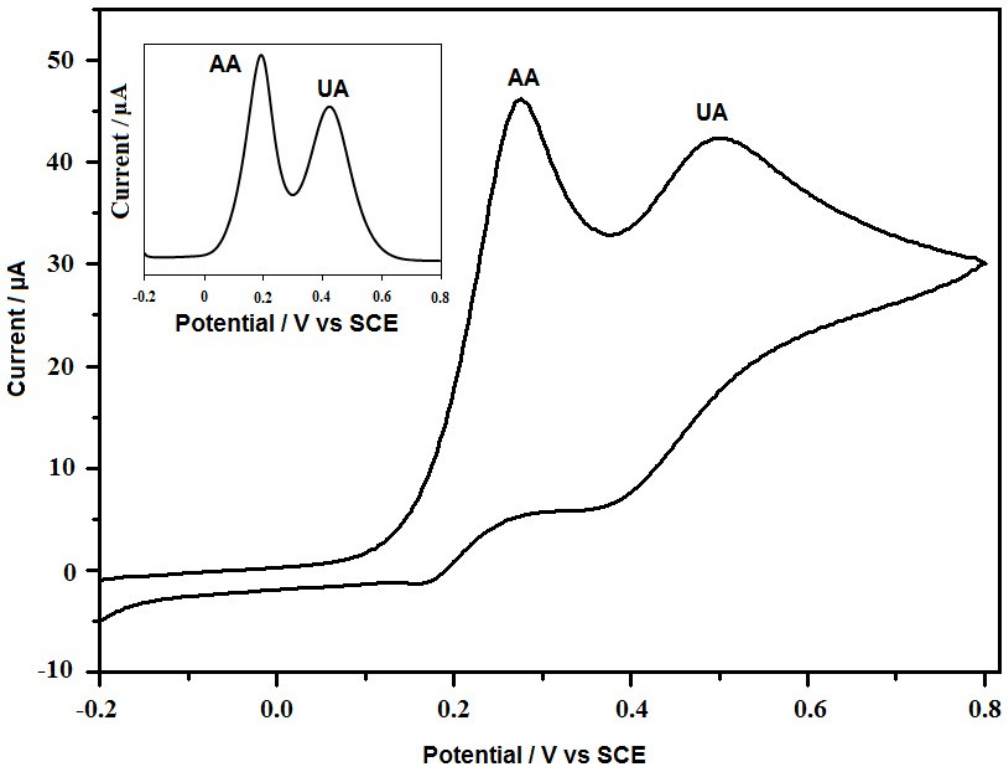

Fig. 13. CVs and DPVs (inset) of 2.0 mM AA and 1.0 mM UA in 0.1 M PBS pH 7.0 in SE-PANI/GCE modified electrode at scan rate 50 mVs^{-1}.

4. Conclusions

SE-PANI nanofibre was prepared by a simple chemical polymerization of aniline using ammonium persulfate (APS) as an oxidant in the presence of hydrochloric acid. FTIR, UV-Visible, XRD, HR-SEM, BET and TG/DTG techniques confirmed the construction of SE-PANI nanofibre. The SE-PANI nanofibre is coated into glassy carbon electrode, and its electrochemical properties were investigated by cyclic voltammetry and electrochemical impedance spectroscopy. The SE-PANI shows enhanced currents in CV and EIS analysis. Finally, SE-PANI nanofibre investigated for uric acid sensor activity. The oxidation peak currents obtained using DPV; the anodic current response was linear with uric acid

concentration on (5.0 x 10^{-5} to 5 x 10^{-3} M). The modified electrode not only improves the electrochemical catalytic oxidation of UA, but also resolves the overlapping anodic peaks of AA and UA. Technical simplicity and possibility of rapid preparation, good reproducibility, high stability, low detection limit (0.104 μM) and wide concentration ranges for UA are the great advantages of this modified electrode. The good electrochemical responses are obtained for seaweed extract doped polyaniline SE-PANI nanofibre. Such novel biosensor provides a promising platform for clinical detection in the future.

Acknowledgements

The authors would like to express our thanks to University Grant Commission, New Delhi, for providing fellowship under UGC-BSR to one of the authors (R.P) and the Department of Industrial Chemistry, Alagappa University for providing HR-SEM analysis.

References

[1] C. R. Raj, F. Kitamura, T. Ohsaka, *Analyst*, 2002, 127, 155–1158.

[2] Y. Ni, D. Cao, S. Kokot, *Anal. Chim. Acta*, 2007, 588,131–139.

[3] R.T. Kachoosangi, C.E. Banks, R.G. Compton, *Electroanalysis*, 2006, 18, 741–747.

[4] N. Cooper, R. Khosravan, C. Erdmann, J. Fiene, J.W. Lee, *J. Chromatogr B*, 2006, 837,1–10.

[5] T. Yamaguchi, K. Hasegawa, S. Kamino, K. Miyachi, H. Tominaga, Y. Fujita, *Anal. Sci.*, 2007, 23, 223–226.

[6] J. Galban, Y. Andreu, M.J. Almenara, S. Marcos, J.R. Castillo, J.R. *Talanta*, 2001, 54,847–854.

[7] D. Yao, A.G. Vlessidis, N.P. Evmiridis, *Anal. Chim. Acta*, 2003, 478, 23–30.

[8] J.M. Zen, P.J. *Chen, Anal. Chem*, 1997, 69, 5087–5093.

[9] S. Schultz, D.R. Smith, J.J. Mock, D.A. Schultz, *Proc Nat Acad. Sci U.S.A*, 2000, 97, 996–1001.

[10] T.A. Taton, C.A. Mirkin, R.L. Letsinger, *Science*, 2000, 289, 1757–1759.

[11] G.V. Ramesh, S. Porel, T.P. Radhakrishnan, *Chem. Soc. Rev*, 2009, 38, 2646–2656.

[12] S.S Gasaymeh, S. Radiman, L.Y. Heng, E. Saion, G.H.M. Saeed, *Afr. Phys. Rev.*, 2010, 4, 31–41.

[13] J. Huang, *Pure Appl. Chem*, 2006, 78, 15–27.

[14] H. Ding, M. Wan, Y. Wei, *Adv. Mater*, 2007, 19, 465–469.

[15] F.R.R. Teles, L.P. Fonseca, *Mater. Sci. Eng. C*, 2008, 28, 1530–1543

[16] D. Plackett, Biopolymers: New Materials for Sustainable Films and Coatings, Wiley, 2011.

[17] V.K. Thakur, M.K. Thakur, *J. Clean Prod*, 2014, 82, 1–15

[18] E. A.O. Fariasa, M.C. Santosa,N. A. Dionisioa, P. V. Quelemesa, J. R.S.A. Leitea, P. Eatonc, D.A. Silvaa, C. Eirasa, *Mater. Sci. Eng. B*, 2015, 200, 9–21

[19] H. Peng, G. Ma, W. Ying, A. Wang, H. Huang, Z. Lei. *J. Power Sources*, 2012, 211:40-45.

[20] M.S. Mansour, M.E. Ossman, H.A. Farag, *Desalination*, 2011, 272, 301-305.

[21] V. Janaki, B.T. Oh, K. Shanthi, K.J. Lee, A.K. Ramasamy S.K. Kannan, *Synth. Met*, 2012, 162, 974-980.

[22] P. Sukitpaneenit, T. Thanpitcha, A. Sirivat, C. Weder, R. Rujiravanit, *J Appl. Polym*. Sci, 2007, 106:4038-4046.

[23] B. Narayan, K. Miyashita, *Indian J. Fisheries*, 2005, 52, 263–268.

[24] S.K. Chandini, P. Ganesan, N. Bhaskar, *Food Chem.*, 2008, 107,707–713.

[25] B. Larsen, D.M.S.A. Salem, M. A. E. Sallam, M. M. Mishrikey, A.I. Beltagy, *Carbohydr. Res.*, 2003, 338, 2325–2336.

[26] D. Leal, B. Matsuhiro, M. Rossi, F. Caruso, *Carbohydr. Res,* 2008, 343, 308–316.

[27] S. Azizi, M.B. Ahmad, F. Namvar, R. Mohamad, *Mater. Lett.*, 2014, 116, 275–277.

[28] S. Bekina, S. Sarmada, K.Gurkanb, G.K. Elic, G. Gurdaga, *Sens. Actuators, B* 2014, 202, 878–892

[29] M. Esch, V.L. Sukhorukov, M. Kurschner, U. Zimmermann, *Biopolymers*, 1999, 50, 227–237.

[30] S. Ikeda, H. Kumagai, K. Nakamura, *Carbohydr. Res*., 1997, 301, 51–59.

[31] S.F. Mohamed, G.A. Mahmoud, M.F.A.Taleb, *Monatsh. Chem*., 2013, 144, 129–137.

[32] A.P. Monkman, P. Adams, *Synth. Met*, 1991, 41, 87–96.

[33] S.X. Xing, C. Zhao, S.Y. Jing, Z.C. Wang, *Polymer*, 2006, 47, 2305–2313

[34] Y. Yu, S. Zhihuai, S. Chen, C. Bian, W. Chen, G. Xue, *Langmuir*, 2006, *22,* 899–3905.

[35] J. Wu L. Yin, *ACS Appl. Mater. Interfaces*, 2011, 3, 4354–4362

[36] Y. Yu, S. Zhihuai, S. Chen, C. Bian, W. Chen and G. Xue, Langmuir, 2006, 22, 3899–3905.

[37] S.J. Su, N. Kuramoto, *Synth. Met.*, 2000, 114, 147–153.

[38] P.S. Khiew, N.M. Huang, S. Radiman, M.S. Ahmad, *Mater. Lett.*, 2004, 58, 516–521.

[39] Y.J. Yu, Z. H. Si, S.J. Chen, C.Q. Bian, W. Chen, G. Xue, *Langmuir*, 2006, 22, 3899-3905.

[40] K.S.W. Sing, D.H. Everett, R.A.W. Haul, L. Moscou, R.A. Pierotti, J. Rouquerol, T. Siemieniewska, *Pure Appl. Chem*, 1984, 57, 603–619.

[41] P. Deepak, A.B. Dubal, V. Sandip, B. Patil, G.S. Gund, D. Chandrakant, B. Lokhande, *J. Alloys Compd*, 2013, 552, 240–247.

[42] G. Wang, L. Zhang, J. Zhang, *Chem. Soc. Rev*, 2012, 41, 797–828.

[43] Y.Q. Dou, Y. Zhai, H. Liu, Y. Xia, B. Tu, D. Zhao, X.X. Liu, *J. Power. Sources*, 2011, 196, 1608–1614.

[44] M.M. Hassan, M. Mueller, M.H Wagners, *J. Appl. Polym. Sci,* 2008, 109:1242–1247.

[45] Y.H. Jang, S.O. Han, I.N. Sim, H.I. Kim, *Composites Part A*, 2013, 47, 83–90.

[46] F. Chen, P. Liu, *Chem. Eng. J*, 2011, 168, 964–971.

[47] L. Shao, J.H. Qiu, H.X. Feng, M.Z. Liu, G.H. Zhang, J.B. An, C.M. Gao, H.L. Liu, *Synth. Met*, 2009, 159,1761–1766.

[48] M. Zhou, J. Guo, L.P. Guo, J. Bai, *Anal. Chem*, 2008, 80, 4642–4650.

[49] J.C. Ndamanisha, X. Bo, L. Guo, *Analyst*, 2010, 135, 621–629.

[50] Y.G. Wang, H.Q. Li, Y.Y. Xia, *Adv. Mater*, 2006, 18, 2619–2623.

[51] H. Mi, X. Zhang, X. Ye, S. Yang, *J. Power Sources*, 2008, 176, 403–409.

[52] M. Zhou, J. Guo, L.P. Guo, J Bai, *Anal. Chem*, 2008, 80, 4642–4650.

[53] J.L. Owens, H.A. Marsh, G. Dryhurst, *J. Electroanal. Chem*, 1978, 91, 231–247.

[54] S.H. Wei, F.Q. Zhao, B.Z. Zeng, *Microchim. Acta*, 2005, 150, 219–224 .

[55] K. Pandiselvi, S. Thambidurai, *Int. J. Biol. Macromol*, 2014, 67, 270–278.

[56] V.Sethuraman, P. Muthuraja, P.Manishankar, *Ana. Methods*, 2013, 5, 6523–6530.

[57] P. Kanchana, C. Sekar, *Mater. Sci Eng., C*, 2014, 42, 601–607.

[58] J. Dua, R. Yuea, Z. Yao, F. Jianga, Y. Du, P. Yang, C. Wang, *Colloids Surf., A*. 2013, 419, 94–99.

[59] C. Wang, J. Du, H. Wang, C. Zou, F. Jiang, P. Yang, Y. Du, *Sens. Actuators B*, 2014, 204, 302–309.

[60] Q. Lian, Z. He, Q. He, A. Luo, K. Yan, D. Zhang, X. Lu, X. Zhou, *Anal. Chim. Acta*, 2014, 823, 32–39.

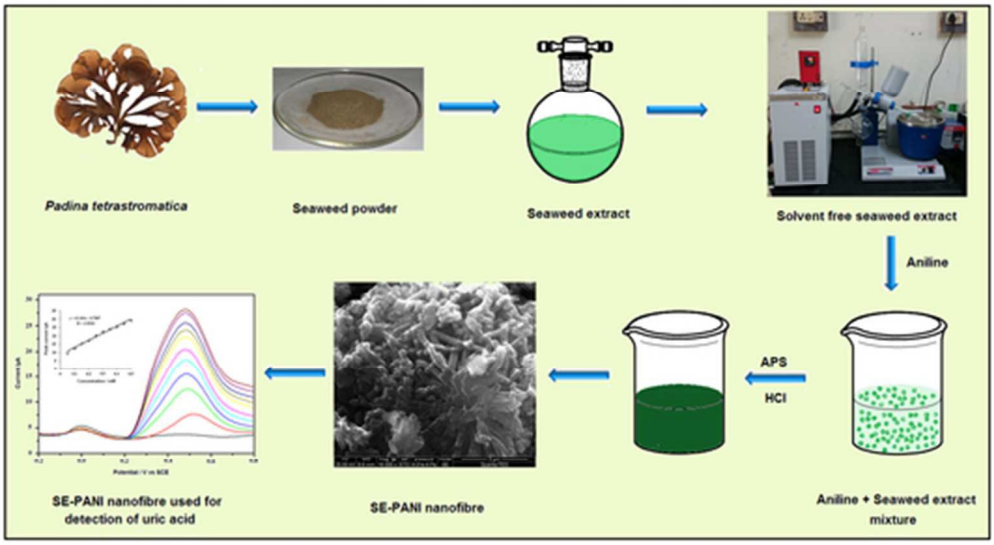

22x12mm (600 x 600 DPI)